TIDAL BEHAVIOUR UNDER AN ANTARCTIC ICE SHELF

J. R. POTTER, J. G. PAREN *and* M. PEDLEY

British Antarctic Survey, Natural Environment Research Council, High Cross, Madingley Road, Cambridge CB3 0ET, UK

ABSTRACT. Two short tidal height records and one short current record are presented. The measurements were taken near the two narrow ice fronts at the north and south ends of George VI Ice Shelf, Antarctic Peninsula. At both ice fronts there is significant tidal height energy in the first seven tidal species, indicating strong non-linear interaction, not all of which can be attributed to shallow-water or frictional terms. In addition, there is severe absorption of tidal energy at the M_2 frequency. Major tidal constituent values are calculated for both ice fronts. Apart from M_2, comparisons with published numerical tidal simulations show good agreement, especially at the northern ice front, which, nevertheless, shows significant differences from the results of a previous tidal record nearby. George VI Sound is shown to be ineffective for tidal transmission. Calculations based on the limited data show that very little tidal energy enters the south of the sound but that rather more propagates into the north. The net tidal energy flux under the shelf is calculated to be only 0.7×10^9 W. Such a low value has important implications for theories of tidal dissipation by ice shelves.

INTRODUCTION

Many aspects of tidal motion on the earth are well understood and accurate temporal predictions have been available for certain sites (usually ports) for centuries. However, there are still areas of tidal research where either more information or a better understanding is needed. For example, there is a dearth of tidal measurements from inhospitable regions such as Antarctica. Schwiderski (1979, 1981*a–e*, 1983) has produced global numerical simulations of the major tides using all reliable tidal data available to him. Schwiderski's maps show where data exist and there are none south of 57° S between 70° W and 160° W. Any measurements within or at the margin of this area would therefore be of value.

An outstanding problem is that of tidal energy dissipation. Of the total tidal power input to the ocean, estimated to be $4.5 \pm 1 \times 10^{12}$ W, less than 50% can be attributed to known dissipative mechanisms (Cartwright, 1978). Schwiderski (1983) proposes that much of the unaccounted power loss is due to the oceanic M_2 tide doing work on the sea bed. Another possible unaccounted energy sink is the tidal flexing of Antarctic ice shelves, as suggested by Doake (1978). Ice shelves are floating ice masses that respond quasi-isostatically to changes in sea level at tidal periods. They are contiguous with ice that is grounded on the land mass of Antarctica and therefore does not move with the ocean tides. Over each tidal oscillation, mechanical energy is required to deform the ice in the transition region between grounded and floating ice. Measurements of the tidal energy flux near ice shelves could help evaluate this type of tidal energy dissipation.

Physical setting

George VI Sound is a narrow channel aligned approximately north–south on the west coast of the Antarctic Peninsula (Fig. 1). It is 500 km long and 25 km wide at its northern entrance widening to roughly 70 km at its southern entrance. The channel is over 1000 m deep in places, cutting into the continental shelf, which lies at 500 m

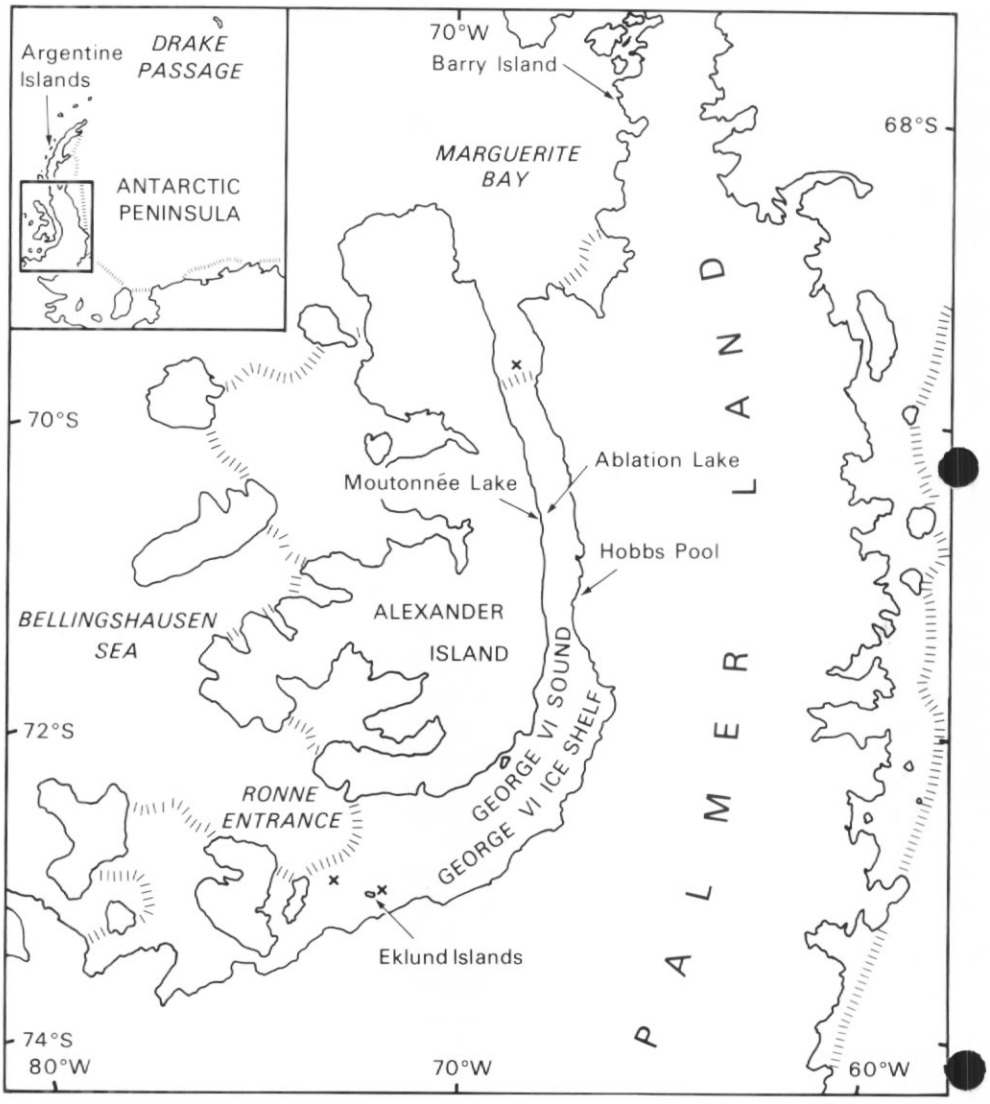

Fig. 1. Map of the Antarctic Peninsula, showing the location of George VI Sound and tidal measurement sites (denoted by crosses).

depth. Most of the channel is occupied by George VI Ice Shelf, which is primarily fed by ice flowing off Palmer Land. The ice shelf thickness, obtained from radio echo sounding (Crabtree, 1983), and the known bedrock topography are shown in Fig. 2. The ice shelf thickens monotonically from 100 m at the northern ice front to 470 m at its maximum just to the east of the Eklund Islands. From this point the ice shelf thins rapidly to only 125 m at the southern ice front. The mean cross-sectional free water depth between the ice shelf base and the sea bottom is approximately 500 m at both ice fronts.

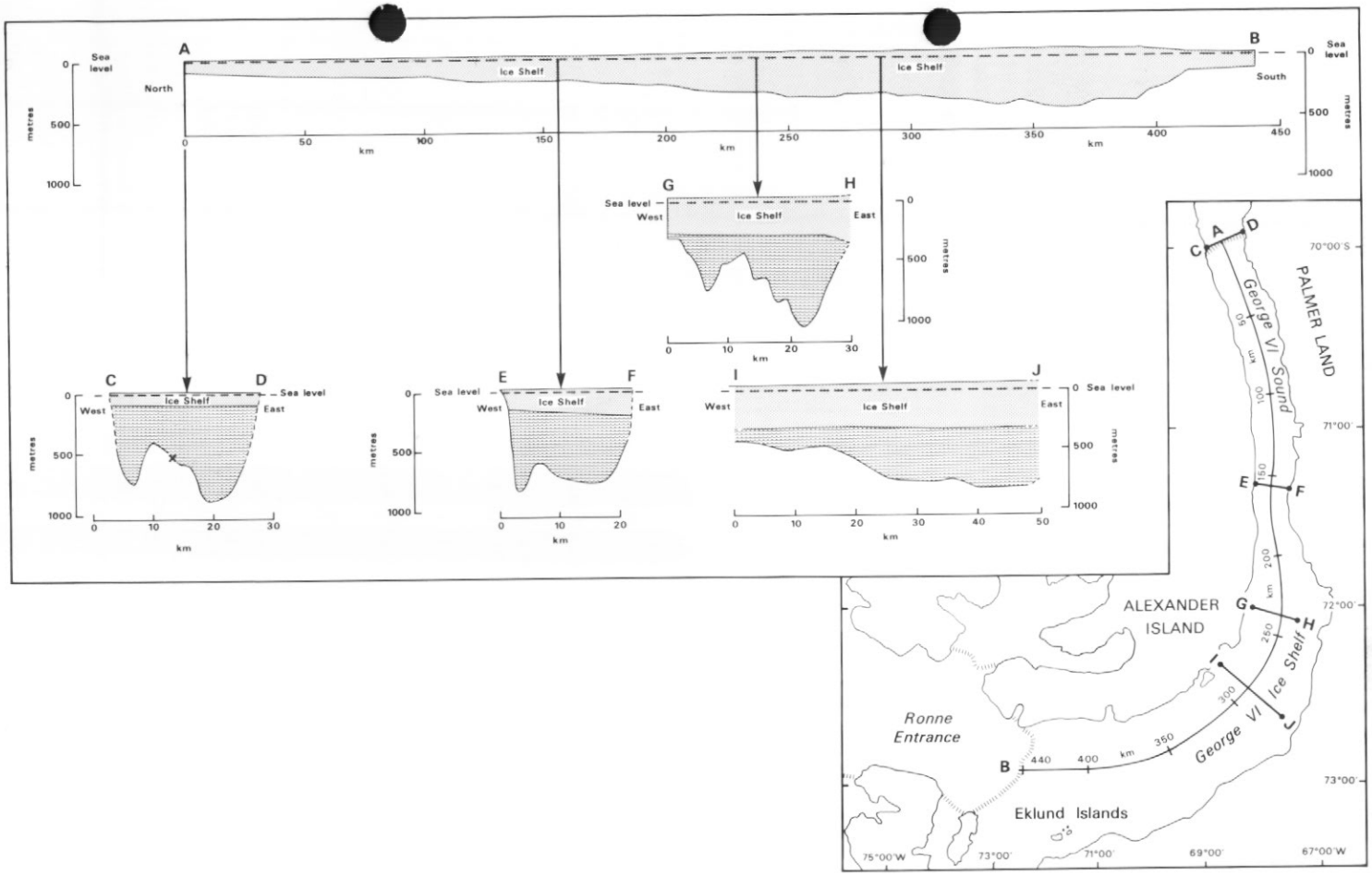

Fig. 2. Ice-shelf thickness on a central line (AB) along George VI Sound and known bedrock topography. Bedrock soundings along the line CD were obtained by plumb line (Loynes and others, 1984), along line GH by seismic shooting (Crabtree and others, 1985) and also along lines EF and IK by seismics (M. Maslanyj, personal communication).

Previous work

Tidal height measurements have been made at the landward margin of the ice shelf in three places: Ablation Lake (70° 49′ S, 68° 25′ W), Moutonnée Lake (70° 52′ S, 68° 23′ W) and Hobbs Pool (71° 18′ S, 67° 35′ W). These sites, which provide access to the sea, are holes in the ice shelf where coastal topography prevents the intrusion of the ice shelf. Ice forms at the surface and becomes frozen to the surrounding ice shelf, moving up and down with it during each tidal cycle. By drilling through the ice and weighting one end of a line on the sea bed, the tidal motion of the ice shelf can be observed. These measurements, together with records from Barry Island (200 km to the north) and Argentine Islands (570 km to the north) have been discussed by Cartwright (1979). In addition, a 156-day record of tidal currents under the ice shelf near the northern ice front is described by Potter and Paren (1985). Schwiderski (1979, 1981*a–e*) used both numerical modelling and available data to provide maps of the major ocean tides. These maps are valuable for comparison with the results from our more recent observations.

Data Collection and Analysis

Short-period measurements of tidal heights and currents are presented for sites near each of the two narrow ice fronts of George VI Ice Shelf. These measurements have been analysed harmonically after the method of Doodson (1921) to obtain the coefficients of the major tidal constituents. Although the response analysis of Munk and Cartwright (1966) is physically more meaningful and should give marginally better results, it requires a more complex set of procedures than the simpler harmonic analysis. From the comparisons of Zetler, Cartwright and Berkman (1979) it was found that a response analysis was not justified for the records presented here. In all cases the shortness of the record has required refinements to be applied to the basic analysis. On the assumption that these are of little interest to those unfamiliar with tidal analysis and common practice to those who are, only brief descriptions of the calculations are given.

The three records presented here consist of:

(1) Tidal height measurements at the Eklund Islands near the southern ice front (45 days).

(2) Current meter data from a rift between the Eklund Islands and the ice front (25 days).

(3) Tidal height measurements from near the northern ice front (16 days).

(1) *Tidal height near the southern ice front*

Sea-bottom pressure was recorded at 10-minute intervals for 45 days from 4 January 1984 by an Aanderaa WLR5 recorder. The meter rested on the sea bed at 212 m depth at 73° 10′ S, 71° 40′ W. Access to the sea was gained by drilling a hole through sea ice that covers a rift in the ice shelf caused by ice flow past the Eklund Islands. The meter was tethered to the surface by a wire, which was used to recover it. The availability of sites in this area is severely restricted by almost continuous ice-shelf cover, 100–200 m thick. The site used was very close to the Eklund Islands group, which causes extensive rifting of the ice shelf. The free water depth near this site varies from nothing where the ice shelf grounds on the island group to 400 m within 20 km north-west towards the southern ice front (Fig. 3). Examination of an ice-depth map (Crabtree, 1983) together with known bedrock topography indicates that there is an appreciable area of shallow water, which leads us to expect some non-linear tidal

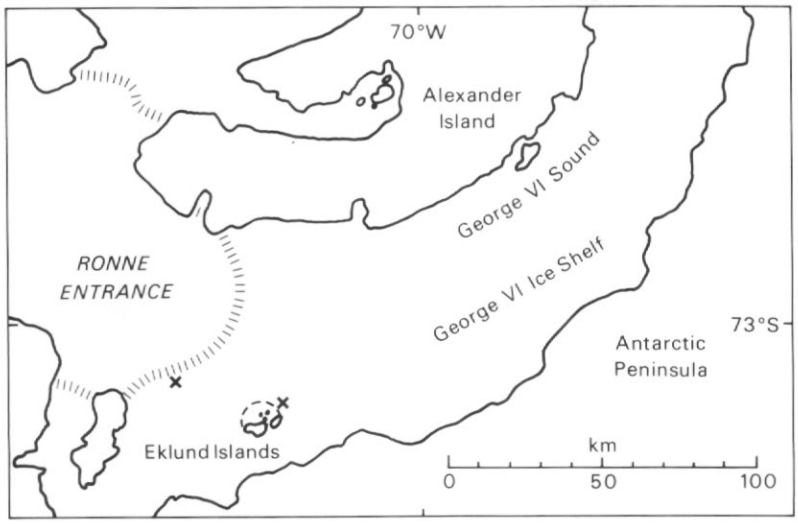

Fig. 3. Southern end of George VI Sound showing the ice front, Eklund Islands and measurement sites (denoted by crosses). The area of open water and sea ice which occupies the rift in the ice shelf near the Eklund Islands is shown by a dashed line.

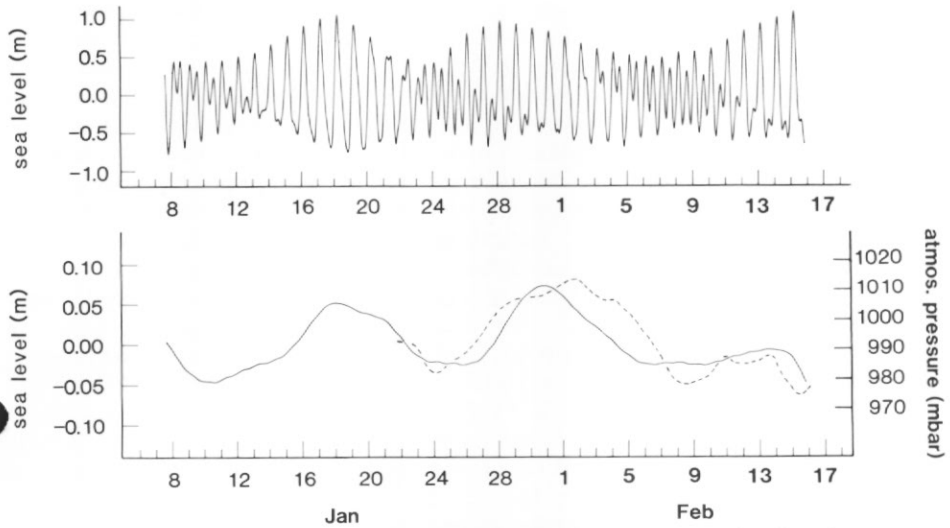

Fig. 4. Plots of the 45-day sea-bed pressure data from the Eklund Islands. The data have been separated into high and low frequency variations and converted to height above mean sea level. Note the very different vertical scales. Some data have been lost at each end of the record during filtering. The high frequency variations are almost purely tidal. A plot of the smoothed atmospheric pressure at the site is shown as a dashed line, for the period during which data is available. The atmospheric pressure scale has been adjusted so that the low frequency variations are of a similar magnitude.

interaction. A plot of the data is shown in Fig. 4, split into higher frequency variations (diurnal and above) and low-frequency changes (with mean sea level subtracted). The very low noise level apparent in Fig. 4 and high data integrity has enabled a rather better tidal analysis than might have been expected for such a short record.

The pressure recorded by the WLR5 is that of the overlying seawater plus the

hydrostatic pressure of the ice shelf and atmospheric pressure. The ice shelf response may not be in equilibrium with the changes in sea level. This possibility does not affect the record because the sum of the sea height and hydrostatic pressure of the ice shelf must always equal that of the sea in the absence of the ice shelf. Had the record been of ice movement, such as for the three lake sites discussed in Cartwright (1979), non-equilibrium behaviour of the ice shelf would have affected the record directly.

Atmospheric pressure variations cause compensatory changes in local sea level, resulting in near constant sea-bed pressure. During large or rapid atmospheric variations, the sea may be unable to compensate fully and a residual pressure signal occurs at the sea-bed. In addition, coastal winds can also cause sea-level changes. The low frequency variations shown in Fig. 4 will include such atmospheric disturbances as well as fortnightly and longer period tides.

The fortnightly tides will include both Mf and MSf. Although Mf has an equilibrium tide very much larger than the true MSf, the non-linear interaction between M_2 and S_2 can cause a fortnightly tide at the MSf frequency. For this reason it is impossible to predict these tides *a priori* and their frequency separation prevents their resolution from this short record. From Cartwright (1979) we might expect an Mf amplitude of some 24 mm with a phase of 230 degrees. This is only half the amplitude of the low frequency variations seen in Fig. 4, and so, in addition, we are led to consider atmospheric causes. A plot of the smoothed atmospheric pressure at the site has been superimposed on the low-frequency bottom pressure in Fig. 4 for the period when both measurements are available. The positive correlation between the two curves is clear, with the main sea-bed pressure peak almost coincident with the atmospheric peak. The atmospheric pressure varies by 35 mbar during the tidal record. An isostatic sea surface response would result in 0.35 m sea-level change. The low-frequency bottom pressure corresponds to a change of 0.1 m, indicating that, if fortnightly tides are ignored, the sea was only able to make 70% of the expected equilibrium response.

A spectral analysis of the raw data is shown in Fig. 5. Energy is present at the 95% confidence level in the first seven tidal species. The higher species tides are due to non-linear coupling of the primary tides, partly caused by tidal propagation over the local topography described above. The 5th and 7th tidal species, however, are not normally expected from frictional or shallow-water terms and indicate that another source of tidal distortion is active. Using the criteria of Godin (1970) the record is only long enough to resolve significant tidal constituents separated by an angular frequency of 0.27 degrees/hour or more. Because of their small amplitude and close angular spacing, it is impossible to evaluate species 3 or higher frequency tides, or to separate close constituent groups such as (P_1, K_1), ($2N_2$, μ_2) or (T_2, S_2, K_2) using a normal harmonic analysis. To overcome this problem for species 1 and 2 tides, a procedure similar to that described in King and others (1983) was used. The method assumes a known amplitude ratio and phase difference between any two tides that cannot be resolved. This constrains the admittance function to be locally smooth. The amplitude ratios and phase differences were inferred from known values near the north of the ice shelf.

King and others (1983) proposed that the time series should be analysed for one of a pair of close tidal frequencies. Amplitudes and phases for both constituents are then inferred from the single amplitude and phase obtained from the first analysis. This method contains an inherent error, which, although small for most applications, increases with the length of the time series. The error arises because, even though the two tides may have a beat period longer than the record, which prevents a resolution of the tides, some beat modulation of the joint amplitude will occur. The subsequent splitting of the resolved energy into two tides then consistently underestimates the amplitudes. Instead, a modified harmonic analysis was done using as constraints the

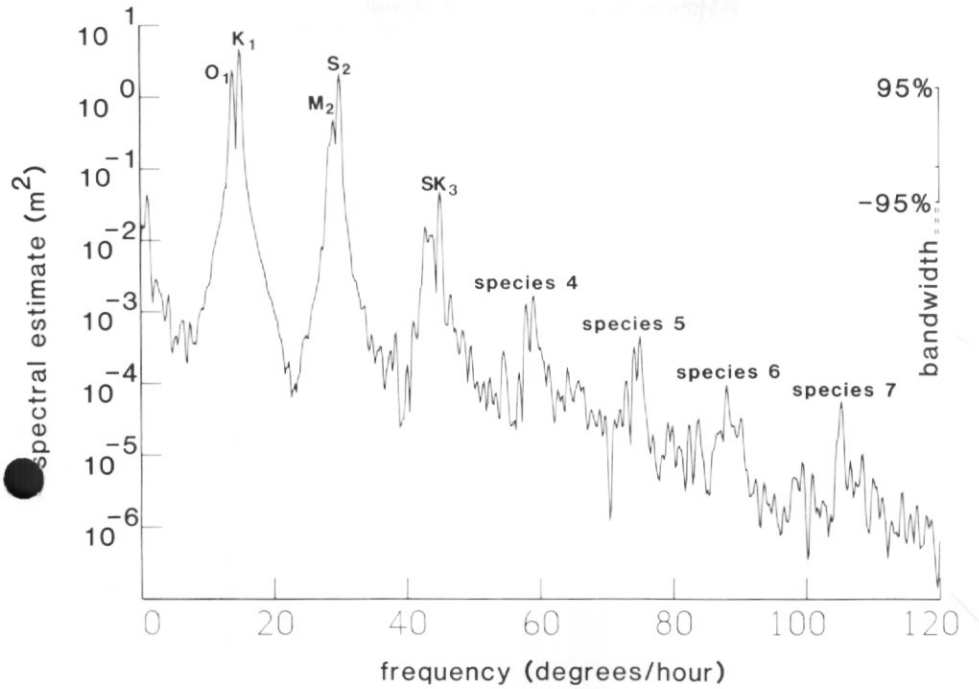

Fig. 5. Spectral plot of the 45-day pressure record. There is a peak corresponding to the low frequency variation shown in Fig. 4 as well as for the first 7 tidal species. The upper and lower 95% confidence limits are shown, with the bandwidth represented by the width of the tick marks. The vertical scale is such that the average value is equal to the variance of the data.

amplitude ratios and phase differences between doublets found at Ablation Lake. The results for the main tidal constituents are shown in Table I. In the frequency range 10-35 degrees/hour, the variance of the data is 0.1650 m² and of the deviation between data and theory, 0.0004 m². Of the variance in this frequency range, 97.5% is therefore accounted for by the tidal prediction.

(2) *Tidal and other currents near the southern ice front*

An Aanderaa RCM4 current meter was suspended from the ice shelf at a depth of 245 m at 73° 09′ S, 72° 49′ W. Sea floor depth is over 720 m at this site. Data were recorded every five minutes for 25 days from 20 January 1984. The site is at a rift in the ice shelf (Fig. 6) filled with a crust of sea ice, which can be penetrated easily. The rift is 6 km from the southern ice front in Ronne Entrance and 30 km from the Eklund Islands (Fig. 3).

Spectral analyses of the flow components in the true north and east directions are shown in Fig. 7. It is apparent that the energy is smoothly distributed with a monotonic rise in energy density towards the lower frequencies. Only the species 2 tides emerge from the energy continuum, suggesting that the species 1 tides must be weaker. Rather more energy is associated with the east–west direction than with the north–south at all frequencies. This reflects the topography of the channel at this site, which is aligned roughly east–west.

The record is too short and the signal/noise ratio is too poor to evaluate accurately the tidal constituents by means of simple harmonic analysis. Instead, a restricted set

Table I. Summary of the tidal heights and currents at the north and south ends of George VI Ice Shelf.

	Eklund Islands area tidal height		*Southern ice front area tidal currents*				*Northern ice front area tidal height*		*Northern ice front area tidal currents*			
			East, into channel		*North, across channel*				*Southerly, into channel*		*Easterly, across channel*	
Constituent	*mm* ±8%	*deg.* ±8	*mm s*$^{-1}$ ±20%	*deg.* ±15	*mm s*$^{-1}$	*deg.*	*mm* ±10%	*deg.* ±10	*mm s*$^{-1}$	*deg.*	*mm s*$^{-1}$	*deg.*
Q_1	58	78	—	—	—	—	58	79	2.6	334	—	—
O_1	270	80	—	—	4.5	254	259	76	12.3	0	2.0	72
P_1	109	94	1.8	316	—	—	107	91	6.1	22	—	—
K_1	327	99	5.3	321	2.0	160	319	93	17.4	26	3.6	91
$2N_2$	21	149	—	—	—	—	—	—	2.9	41	—	—
μ_2	23	153	—	—	—	—	—	—	2.9	51	—	—
N_2	90	161	3.4	99	—	—	70	158	10.8	64	3.4	106
M_2	131	271	12.9	206	9.6	331	124	267	10.0	168	2.3	275
L_2	29	70	—	—	—	—	—	—	—	—	—	—
S_2	300	92	10.9	24	8.8	162	220	78	38.7	20	12.5	125
K_2	81	93	2.7	26	2.2	164	57	79	10.7	12	2.9	125

Fig. 6. The rift near the Eklund Islands used for the 25-day current meter mooring. The ice shelf is too thick to penetrate but the sea ice filling the rift is much thinner and provides a stable working platform.

of constituents was used in a harmonic analysis, which employed the method described earlier to separate (P_1, K_1) and (S_2, K_2). T_2 was assumed negligible. Individually, the results are subject to large errors but they should be useful in providing an approximate prediction of tidal flow in the area, to be used in a later section of this paper. The main tidal constituent values obtained are shown in Table I.

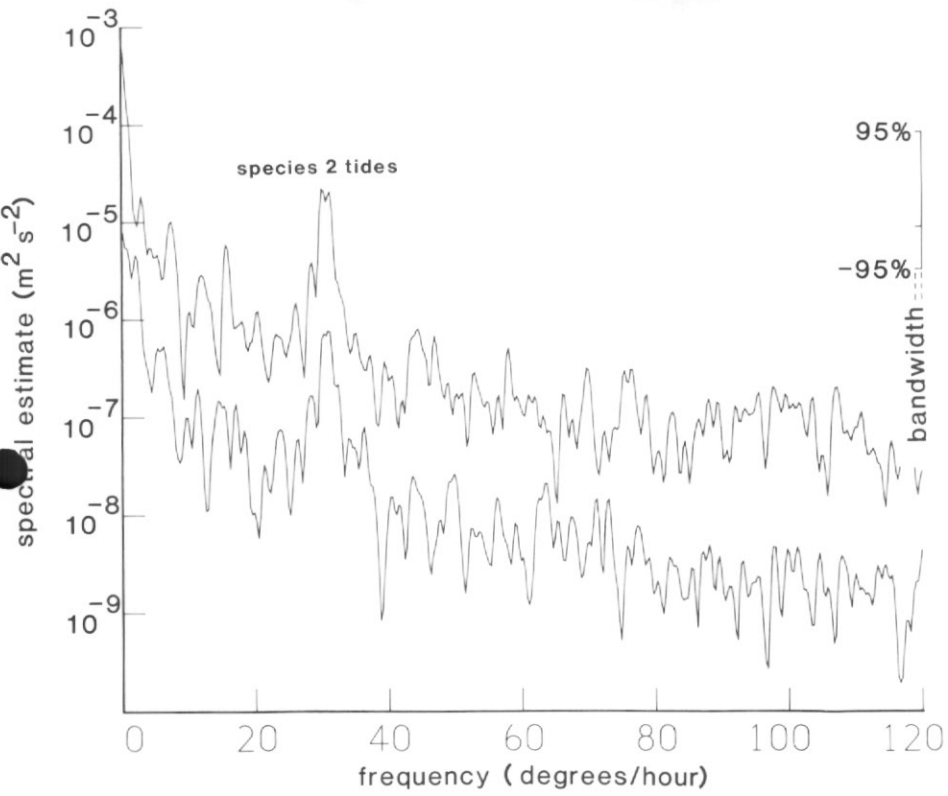

Fig. 7. Spectral analysis of the 25-day current meter record. The upper curve is the east–west current flow and the lower curve (depressed by 10^{-1} for clarity) is the north–south flow. The 95% confidence limits and bandwith are indicated. Only the semi-diurnal tides significantly exceed the background energy level. The vertical scale is such that the average value is equal to the variance of the data.

An interesting feature of the current record is the progressive vector plot (Fig. 8). After the first half of the record, culminating in the period of slack current around 1 February, the progressive vector resolutely aligns itself along 240 degrees clockwise from true north, 40 degrees off the axis of the channel in a direction heading out of George VI Sound into Ronne Entrance. The driving mechanism for this flow has yet to be investigated.

(3) *Tidal height near the northern ice front*

Sea-bottom pressure was recorded at 5-min intervals for 16 days from 3 December 1984 by an Aanderaa WLR5 meter resting on the sea bed 512 m below sea level at 69° 58′ S, 68° 51′ W. The meter was lowered to the sea-bed through 5-m-thick sea ice $\frac{1}{2}$ km north of the ice front in the centre of the channel (Profile CD of Fig. 2). The free water depth exceeds 300 m in this region. Therefore, although the record is too short to analyse accurately for ter-diurnal and higher frequency non-linear tides, we would expect them to be less noticeable than at the southern site near the Eklund Islands discussed earlier, which has much shallower water depths. This expectation is not borne out by the spectral analysis of the data (Fig. 9), which clearly shows energy

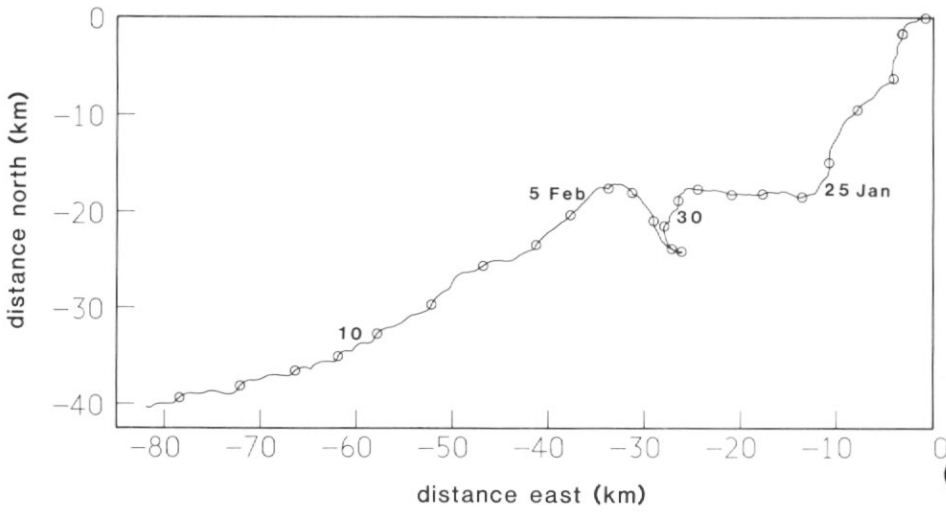

Fig. 8. Progressive vector plot of the 25-day current record from near the southern ice front. The starting point is at the top right-hand corner. 24 hour periods are denoted by circles. Dates are shown beside some parts of the curve. The large cusp corresponds to the high pressure event shown in Fig. 4. Diurnal tidal cusps can just be made out.

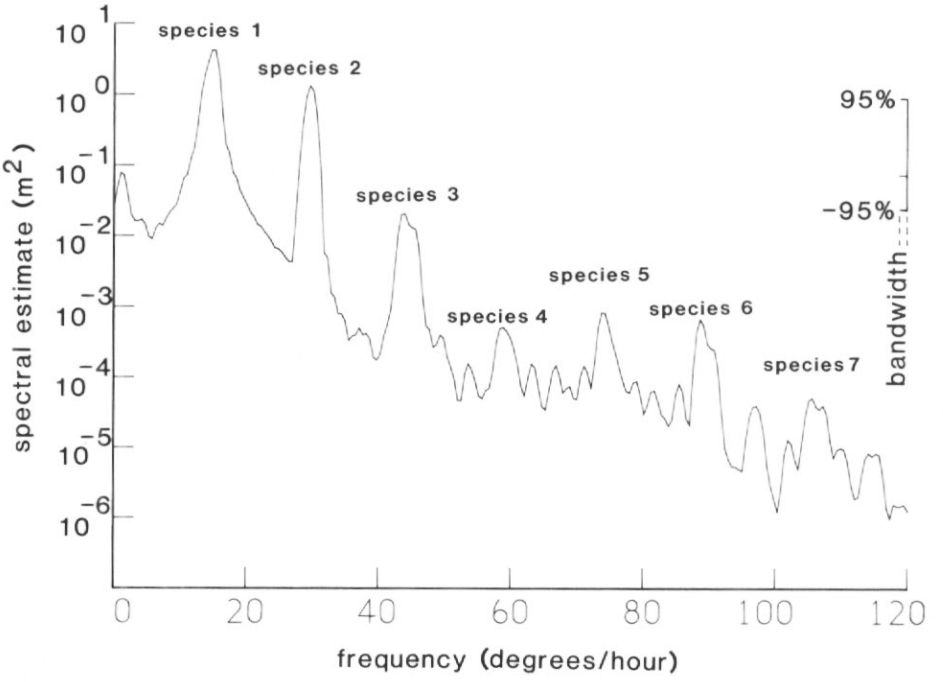

Fig. 9. Spectral analysis of the 16-day sea-pressure record from near the northern ice front. The bandwidth resolution has been sacrificed in order to provide the same 95% confidence limits as for the 45-day spectral plot in Fig. 5. The vertical scale is such that the average value is equal to the variance of the data. The low frequency peak due to atmospheric driving and the first seven tidal species are clearly present.

at the 95% confidence level in the first seven tidal species. The reason may be that the higher species tides are excited not only by shallow-water topography but also by a non-linear response of the ice shelf. Compared with the spectral plot for the Eklund Islands tidal height (Fig. 5), species 4 tides are slightly suppressed and species 6 appears enhanced. The semi-diurnal tides are also suppressed with respect to the diurnals, a result confirmed in the later harmonic analysis.

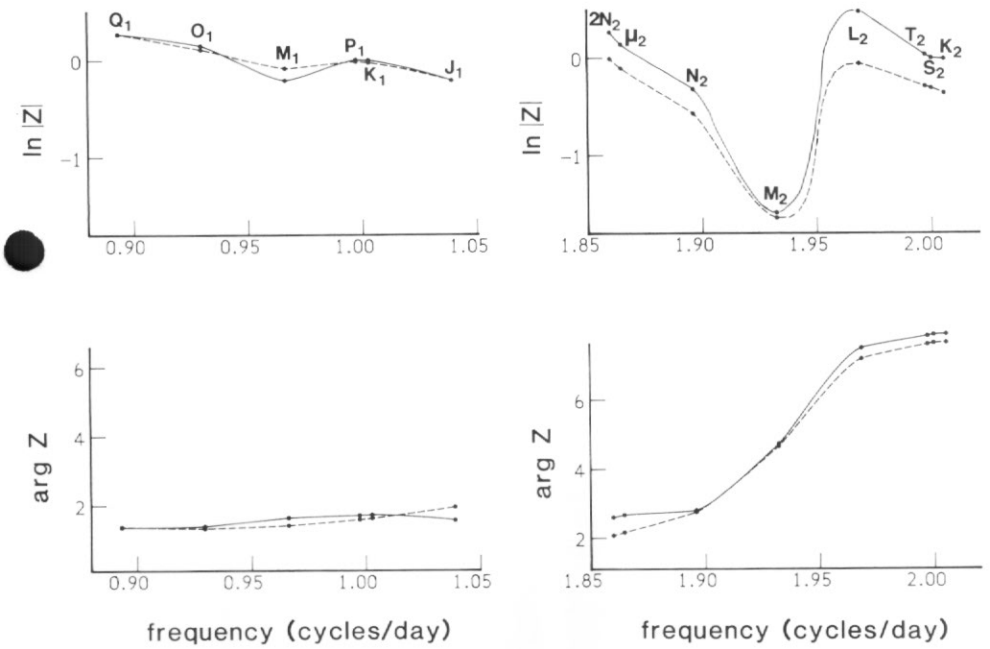

Fig. 10. The admittance, Z, estimated from the major tidal height constituents near the northern ice front (dashed line) and the Eklund Islands (solid line). The frequencies of the tidal constituents used have been annotated in the upper diagrams. The upper half of the diagram shows natural logarithms of the amplitude; the lower, phases in radians. Diurnal frequencies are on the left, semi-diurnal on the right.

As the record was too short to permit a harmonic analysis, it was related to predictions for the same period for Barry Island and Ablation Lake, whose coefficients were determined by Cartwright (1979), and to an Eklund Islands prediction from the coefficients determined above. In each case, a least-squares optimization between prediction and data was performed by the variation of four parameters. These parameters were a phase lag and an amplitude multiplication factor for both the diurnal and semi-diurnal frequency bands. The results showed that, with the two phase lags and amplitude attenuations applied independently for each site, the Eklund Island constituents were able best to mimic the recorded tidal height at the northern ice front. The Ablation Lake values were not so close and the Barry Island values were clearly the least similar to the northern ice front. Using a bandpass filter to restrict the frequency range to the diurnal and semi-diurnal bands, a least-squares method was used to obtain the best linear combination of the estimates obtained from the correlations with the known sites. Within this restricted frequency range, the variance of the data is 0.1420 m^2 of which 96.5% is accounted for by the tidal prediction, leaving

a residual variance of only 0.0005 m^2. The results from this analysis are shown in Table 1. The modulus and argument of the admittance function, estimated from the constituent values in the diurnal and semi-diurnal bands, are shown in Fig. 10 with those for the Eklund Islands tidal height.

Comparison of Results

The admittances plotted in Fig. 10 clearly indicate that the tidal heights at both ends of George VI Sound are of a very similar character. This is not surprising because the constituents for the northern ice front were calculated with constraints equivalent to insisting on a smooth admittance function with a character made up from those of three nearby sites (Eklund Islands, Ablation Lake and Barry Island). Even so, the low unaccounted variance in the diurnal and semi-diurnal bands leads us to believe that these were reasonable constraints and that the curves plotted in Fig. 10 are good representations of the admittances. As expected from the spectral analysis, the northern semi-diurnal amplitudes are attenuated by approximately 20% compared to the southern values whereas the diurnal amplitudes are very similar. In both cases the diurnal tidal amplitudes exceed the semi-diurnal, in contrast with the tidal current behaviour in the south (Fig. 7) and north (Potter and Paren, 1985).

The most striking feature of the admittances is the severe attenuation of energy at frequencies near M_2. This attenuation is associated with a 320-degree change in phase and a tidal age of 7 days. Cartwright (1979) also found a tidal age of 7 days at Ablation Lake, 90 km south of the northern ice front. The tidal age is the time elapsed between the new or full moon and the observed spring tide and is indicated by the phase lag between M_2 and S_2 (Cartwright, 1978). Webb (1973) has attributed tidal ages of 60 h or more to tidal energy dissipation, usually in the shallow water over continental shelves. Webb (1982) specifically associates large energy losses with the west coast of the Antarctic Peninsula where tidal ages are of the order of 4–7 days. This large tidal age, twice that commonly encountered in shelf seas, may be due to the tidal energy dissipation by ice shelves. If this is correct, the ice shelf response to tidal forcing causes the sharp attenuation in the M_2 energy. It is difficult to explain why ice-shelf energy absorption should produce such a finely tuned response or why there is an equally sharp attenuation at the neighbouring frequency of N_2 at Argentine Islands, remote from Antarctic ice shelves.

A comparison of phases in Table I shows that the Eklund Islands diurnal tide lags that at the northern ice front by 4 degrees (mean weighted by amplitude). The semi-diurnal tide lags by 10 degrees. These phase lags would represent approximately 18 minutes time difference between the tide at the north and south of George VI Sound. This is only 20% of the time required for a simple progressive wave of tidal period to propagate down the channel from north to south. The conclusion is that the tide cannot propagate through the channel but rather arrives independently at each end from a north-westerly direction.

A conflict occurs between the observed phases at the northern ice front and those reported by Cartwright (1979) for Ablation Lake, 90 km to the south. For the diurnals, Ablation Lake shows phase 4 degrees in advance of the northern ice front and for the semi-diurnals, 1 degree. For a simple progressive wave propagating southwards as suggested by Cartwright (1979), one would expect phase lags of 5 and 10 degrees respectively rather than the slight leads observed. Cartwright estimates a phase error in his results of ± 3 degrees. We estimate our error to be ± 10 degrees. The discrepancy is thus just within the individual combined error expectation but is unlikely to occur, as it does on average, over all the tidal constituents. Cartwright

(1979) noted that the constituent values for Moutonnée Lake are very different from the Ablation Lake results, only 10 km to the north. He attributed this result to the poor quality of the Moutonnée Lake record and considerable lateral variation in the tidal movement of fast ice. There are problems associated with making tidal measurements from ice platforms, as described by Bishop and Walton (1977), which was the method used to obtain the records analysed by Cartwright. There is also a suspected difference between ice shelf motion and unrestrained sea level response to tidal forcing. These are the most likely causes of the phase conflict between Cartwright's results and our own.

Table II. Comparison of observed major tides with predictions from numerical simulations

Constituent	*Eklund Islands area tidal height*		*Schwiderski prediction for near Eklund Islands*		*Northern ice front area tidal height*		*Schwiderski prediction for near northern ice front*	
	mm	*deg.*	*mm*	*deg.*	*mm*	*deg.*	*mm*	*deg.*
O_1	270	80	300	93	259	76	250	79
P_1	109	94	140	103	107	91	100	94
K_1	327	99	500	104	319	93	320	94
N_2	90	161	80	188	70	158	60	159
M_2	131	271	210	326	124	267	180	272
S_2	300	92	330	95	220	78	190	76

Platzman (1984) cites five of the most recent global models of the M_2 tide. Of these, only Schwiderski's (1979, 1983) and Zahel's (1977) have sufficient resolution to be useful for comparison with our observations. Zahel (1977) uses bottom friction and eddy viscosity to dissipate 3.8×10^{12} W, rather more than currently estimated for these processes (Cartwright 1978). Lambeck (1977) indicates that Zahel's eddy viscosity value is too large. Schwiderski (1983) uses a bottom friction dissipation of only 1.9×10^{12} W with negligible eddy dissipation. Furthermore, he has produced global models for all the major ocean tides (O_1, P_1, K_1, N_2, M_2, S_2), so we have taken his models for comparison with our observational results. Schwiderski (1983) gives a revision of his earlier M_2 tidal simulation but, for our purposes, it appears identical to that in Schwiderski (1979). The original series of models (Schwiderski 1979, 1981*a–e*) have therefore been used for our comparisons. Table II shows our values calculated from observations and values obtained for the same sites by extrapolation from Schwiderski's simulated values. Comparison of the two sets of values for the northern ice front shows remarkably good agreement. Diurnal amplitudes differ by 2%, semi-diurnals by 15% and phases in both frequency bands by only 2 degrees. Comparison of results for the Eklund Islands shows a poorer agreement. Observed diurnal amplitudes are 25% less than for Schwiderski's prediction and phases lead Schwiderski's by 8 degrees. In the semi-diurnal band our amplitudes compare well with Schwiderski's and are within 10% but again the phases lead the simulation, in this instance by approximately 10 degrees.

The above comparisons have been made excluding M_2. This constituent shows an amplitude 31% less in the north and 37% less in the south than in Schwiderski's simulation. The observed phase leads the simulation by 5 degrees in the north and 55 degrees in the south. The indication is that the simulation does not fully reproduce the severe attenuation of the admittance in the region of M_2. At other tidal frequencies

the agreement is generally good, with an excellent match for the north of George VI Sound. Schwiderski's simulation includes the effects of eddy dissipation, shallow water effects and bottom friction on tidal energy. Its generally good agreement with our observations, contrasting with the M_2 disparity, further supports the suggestion that the M_2 attenuation is connected with ice shelf energy dissipation, an effect understandably omitted from Schwiderski's simulation.

Schwiderski's models use 1°-square grid elements. On this scale, the coastline in the simulation connects Alexander Island with the Antarctic Peninsula, denying the existence of George VI Sound. That this omission has only a marginal, if any, deleterious effect on the simulation confirms that tidal energy flow through the channel is unimportant. This agrees with the earlier deduction from comparing observed phases at the north and south.

Tidal Energy Fluxes

Tidal energy comes from the gravitational force between the earth and other bodies in the solar system. The rotation of these bodies results in an equipotential surface on the earth that is not geostationary. As a result, tidal energy is dissipated in the relative motion between the earth and, primarily, the sea, which tends to follow the equipotential surface. The main processes that have been identified as oceanic tidal energy sinks are due to eddy viscosity and sea bottom friction. Schwiderski (1983) suggests that a further process, oceanic work done on the lithosphere, provides another major energy sink and Platzman (1984) proposes several other tenable hypotheses. These energy losses cause torques on the earth, sun and moon, which change the angular velocities of these bodies.

The lunar angular acceleration can be calculated from astronomical observations, leading to an estimate for the total M_2 energy dissipation of the oceans. Estimates for this contribution range from 3.0 to 3.8×10^{12} W. Cartwright (1978) suggests an average of $3.2 \pm 0.15 \times 10^{12}$ W based on the most recent review by Lambeck (1977). This value considerably exceeds the total energy loss that can be positively ascribed to M_2 dissipation in the sea, some $1.5 \pm 0.9 \times 10^{12}$ W (Lambeck, 1977). It is therefore an outstanding problem to identify which of the suggested mechanisms is responsible for the dissipation of the remaining tidal energy.

Doake (1978) suggested that Antarctic ice shelves may be responsible for nearly all of the unaccounted energy loss (perhaps up to 2×10^{12} W for all the tides). His calculation was based on the energy required to deform ice shelves at their grounding lines where the ice first becomes afloat on the sea. Since the floating ice must respond to the tidal height changes of the sea surface and the grounded ice must remain stationary, some energy will be lost in each tidal cycle. A problem arises in the calculation because it is difficult to establish the stress–strain relationship for this type of deformation.

One way of assessing the importance of ice shelf deformation is to calculate the tidal energy flux under ice shelves directly. The energy flux per unit area perpendicular to the direction of propagation is given by

$$\tfrac{1}{2}\rho g \int u\eta \cos\theta \, \mathrm{d}w, \tag{1}$$

where ρ is the density of water, $g = 9.82$ m s^{-2}, u is the tidal current amplitude, η is the tidal height amplitude and θ is the phase difference between the tidal flow and height at frequency w. The integration is over tidal frequencies. To calculate the total tidal energy flux into an ice shelf would require an integration of this expression over a surface which separates the ice shelf from the sea. For most ice shelves, which have

extensive contact with the sea provided by a long ice front, the lack of data and the size of program needed to acquire it makes this task unattractive.

George VI Ice Shelf provides a much simpler setting because it connects with the sea only through two narrow ice fronts. The channel is steep sided and deep (Fig. 2), so shallow water coastal effects should be small. Away from shallow water, tidal height should vary little over distances of 50 km or so, allowing tidal height at one site to be extrapolated reasonably along an ice front. The tidal height will, therefore, be assumed constant over each of the ice fronts. Tidal current behaviour, however, is less well known. There is no reason to suspect that the tidal currents vary appreciably across the ice fronts but there is almost certainly some variation with depth.

Prandle (1982) has studied the vertical structure of tidal currents in the absence of ice cover and has established the range of possibilities. In all cases, phase increases towards the sea bed. Tidal amplitude generally remains approximately constant for the upper half of the water column and then decreases towards the bottom. In George VI Sound the bottom surface of the floating ice shelf will present another source of friction in addition to that encountered at the sea bed. We expect this additional friction to alter the phase and amplitude near the bottom surface of the ice shelf in much the same way as sea-bed friction does at the sea floor. Our current measurements were taken comparatively close to the level of the bottom surface of the ice shelf. A detailed application of Prandle's results is therefore not justified; his model needs first to be extended to allow for an ice cover on the sea surface. We cannot say whether the phases and amplitudes will be greater or less than the depth mean values. We estimate that the effect of ignoring the depth-dependence of tidal currents in our calculations is to introduce an uncertainty of some 20% in amplitude and 15 degrees in phase. We continue with an estimate of the tidal energy flux at both ice fronts.

(1) *Southern ice front*

Table I gives the tidal heights and currents for the southern ice front area. The height and currents are from sites 30 km apart but the major tidal constituent heights are not expected to vary greatly over this distance. A more serious problem is the sparsity of reliable tidal current values. This is not only because of the shortness of the record from which they were calculated but also because the currents are so weak. For a simple progressive shallow water wave, the current amplitude is given by

$$u = \eta(g/h)^{\frac{1}{2}},$$

where h is the free water depth. This calculation gives values 8 times too large for the diurnals and 3 times too large for the semi-diurnals. It is immediately apparent, therefore, that the southern ice front does not experience a simple progressive tidal wave. Estimating the tidal energy flux by equation 1 gives a weak energy flux roughly to the west for the diurnals and to the east for the semi-diurnals. The effective width of the channel at this point was taken to be 60 km and the free water depth to be 600 m. The net flux for both tidal species is then 0.2×10^9 W towards 46 degrees east of true north, into the channel. Due to the uncertainty of the current amplitudes, the tidal flux is vulnerable to large error. The only certainty is that the total energy flux at the southern ice front is undoubtedly small.

(2) *Northern ice front*

Both tidal height and currents were measured at the same site at the northern ice front, centrally in the channel. The values are shown in Table I. The current values

were derived from 156 days of data previously presented in Potter and Paren (1985). All the constituents show a significant standing wave component. The easterly currents may be disregarded because the channel is only 25 km wide at this site and Table I shows the easterly flow to be minimal. The tidal energy is southwards into the channel for both diurnal and semi-diurnal tides. Taking the width of the channel to be 25 km and the free water depth to be 500 m gives a net energy flux of 0.5×10^9 W southwards into the channel. Of the energy flux, 87% is provided by K_1 and S_2 alone. The transmission is only 37% of the optimum for a fully progressive wave.

In total, the northern and southern ice fronts allow a tidal energy flux of 0.7×10^9 W to pass into the channel. We estimate that this result could be subject to an error of 0.4×10^9 W.

Comparison of energy fluxes

Doake (1978) gives an equation to calculate the tidal energy absorption of ice shelves at their grounding line given that the deformation is that of transient creep with parabolic strain hardening. The equation predicts a total tidal energy dissipation of approximately 2×10^{12} W for Antarctica. This is larger than the energy dissipated by all the shallow seas and would account for nearly all the unexplained tidal energy loss. The equation depends on the tidal frequency and height amplitude and on the ice thickness at the grounding line. The expected energy dissipation for George VI Ice Shelf alone was calculated for O_1, K_1 and S_2 by dividing the grounding line into six characteristic regions that were each considered to have a constant ice thickness estimated from a recently published radio echo map (Crabtree, 1983). Tidal heights from the northern and southern ice fronts and from Ablation Lake were used in the calculation. In total, the expected tidal energy dissipation from Doake's analysis is 1.2×10^{10} W. This figure is 16 times that of the total energy flux entering the channel calculated from our observations.

Although there may be considerable error in our calculations of the observed energy flux, especially for the southern ice front, such a disparity between Doake's model and our observations cannot be accommodated. It may be that George VI Ice Shelf absorbs an atypically small amount of tidal energy. The ice shelf is unusual in that the grounding line is rather long compared to the area of the ice. Also, the tidal range may be smaller in the central areas than near the ice fronts. In addition, there may be difficulties in applying the energy dissipation formulae. Holdsworth (1977) notes that many ice shelves have a concavity in their basal surface close to the grounding line resulting in an appreciable thinning there. Holdsworth also suggests that tidal motion should create cracks in the top and bottom surfaces of the ice shelf, considerably relieving the stress in these areas. For these reasons, the expected energy absorption calculated from Doake's analysis may be unreasonably high. Even so, it seems unlikely that these effects could produce such a large difference between predicted and observed energy absorption rates. We are therefore drawn to the conclusion that a basal concavity together with surface and bottom crevassing may reduce energy dissipation significantly. Transient creep may also be inappropriate mechanism for ice-shelf grounding-line flexure at tidal frequencies. If the tidal energy absorption of other Antarctic ice shelves were similarly reduced from Doake's estimate, the total tidal energy loss due to this mechanism would be approximately 0.1×10^{12} W.

Conclusions

The two sea height records presented have provided good values for tidal height at both ice fronts of George VI Ice Shelf. The numerical simulations of Schwiderski have been shown to be in good agreement, except for the M_2 constituent. Significant energy has been found in the first seven tidal species. Not all of this can be attributed to non-linear interaction due to shallow water. The indication is that some of the higher species tidal energy is caused by a non-linear response of the ice shelf to tidal forcing. The tidal height observations are consistent with zero tidal propagation down George VI Sound. A crude calculation of tidal energy flux into the sound indicates that only 0.7×10^9 W is absorbed by the ice shelf and other mechanisms in the sound. Unless George VI Ice Shelf is atypical in the way its grounding line absorbs tidal energy, the result cannot be reconciled with Doake's predicted energy absorption based on transient creep. If other ice shelves absorb correspondingly less tidal energy, the ice shelf energy absorption for the whole of Antarctica is estimated to be some 0.1×10^{12} W about 10% of that due to shelf sea dissipation throughout the world.

Acknowledgements

The authors would like to thank Jack Tighe for his sterling efforts in the field as an able and resourceful assistant.

Received 15 March 1985; accepted 30 April 1985

References

Bishop, J. F. *and* Walton, J. L. W. 1977. Problems encountered when monitoring tidal movement in extremely cold conditions. *Polar Record*, **18**, 502–5.

Cartwright, D. E. 1978. Oceanic tides. *International Hydrographic Review*, **55**, 35–84.

Cartwright, D. E. 1979. Analyses of British Antarctic Survey tidal records. *British Antarctic Survey Bulletin*, No. 49, 167–79.

Crabtree, R. D. (*compiler*). 1983. *British Antarctic Territory ice thickness map*, 1:500000. *Sheet 1, edn. 1, Alexander Island.* Cambridge, British Antarctic Survey.

Crabtree, R. D., Storey, B. C. *and* Doake, C. S. M. 1985. The structural evolution of George VI Sound, Antarctic Peninsula. *Symposium on geophysics of the polar regions: XVIII general assembly of the International Union of Geodesy and Geophysics, Hamburg, 15–27 August 1983.* (In press.)

Doake, C. S. M. 1978. Dissipation of tidal energy by Antarctic ice shelves. *Nature*, **275**, 304–5.

Doodson, A. T. 1921. The harmonic development of the tide generating potential. *Proceedings of the Royal Society, Series A*, **100**, 306–28.

Godin, G. 1970. The resolution of tidal constituents. *International Hydrographic Review*, **47**, 133–44.

Holdsworth, G. 1977. Tidal interaction with ice shelves. *Annales de Géophysique*, **33**, 133–46.

King, H. L., Scott, M. A. *and* Smith, T. J. 1983. Some remarks on the analysis of short tidal records. *Deutsche Hydrographische Zeitschrift*, **36**, 45–59.

Lambeck, K. 1977. Tidal dissipation in the oceans: astronomical, geophysical and oceanographic consequences. *Philosophical Transactions of the Royal Society, Series A*, **287**, 545–94.

Loynes, J., Potter, J. R. *and* Paren, J. G. 1984. Current, temperature and salinity beneath George VI Ice Shelf, Antarctica. *Deep-Sea Research*, **31**, 1037–55.

Munk, W. H. *and* Cartwright, D. E. 1966. Tidal spectroscopy and prediction. *Philosophical Transactions of the Royal Society, Series A*, **259**, 533–81.

Platzman, G. W. 1984. Normal modes of the world ocean. Part IV. Synthesis of diurnal and semidiurnal tides. *Journal of Physical Oceanography*, **14**, 1532–50.

Potter, J. R. *and* Paren, J. G. 1985. Interaction between ice shelf and ocean in George VI Sound, Antarctica. (*In* Jacobs, S. S. *ed. Oceanology of the Antarctic continental shelf. Antarctic Research Series*, Vol. 43. Washington DC., A.G.U.) (In press.)

Prandle, D. 1982. The vertical structure of tidal currents and other oscillatory flows. *Continental Shelf Research*, **1**, 191–207.

SCHWIDERSKI, E. W. 1979. Global ocean tides part II. The semidiurnal principal lunar tide (M_2), atlas of tidal charts and maps. *Naval surface weapons center report*, No. NSWC TR 79–414.

SCHWIDERSKI, E. W. 1981*a*. Global ocean tides. Part III. The semidiurnal principal solar tide (S_2), atlas of tidal charts and maps. *Naval surface weapons center report*, No. NSWC TR 81–122.

SCHWIDERSKI, E. W. 1981*b*. Global ocean tides. Part IV. The diurnal luni-solar declination tide (K_1), atlas of tidal charts and maps. *Naval surface weapons center report*, No. NSWC TR 81–142.

SCHWIDERSKI, E. W. 1981*c*. Global ocean tides. Part V. The diurnal principal lunar tide (O_1), atlas of tidal charts and maps. *Naval surface weapons center report*, No. NSWC TR 81–144.

SCHWIDERSKI, E. W. 1981*d*. Global ocean tides. Part VI. The semi-diurnal elliptical lunar tide (N_2), atlas of tidal charts and maps. *Naval surface weapons center report*, No. 81–218.

SCHWIDERSKI, E. W. 1981*e*. Global ocean tides. Part VII. The diurnal principal solar tide (P_1), atlas of tidal charts and maps. *Naval surface weapons center report*, No. 81–220.

SCHWIDERSKI, E. W. 1983. Atlas of ocean tidal charts and maps, Part I. The semidiurnal principal lunar tide M_2. *Marine Geodesy*, **6**, 219–65.

WEBB, D. J. 1973. On the age of the semi-diurnal tide. *Deep-Sea Research*, **20**, 847–52.

WEBB, D. J. 1982. Tides and tidal energy. *Contemporary Physics*, **23**, 419–42.

ZAHEL, W. 1977. A global hydrodynamic-numerical 1°-model of the ocean-tides; the oscillation system of the M_2-tide and its distribution of energy dissipation. *Annales de Géophysique*, **33**, 31–40.

ZETLER, B. D., CARTWRIGHT, D. E. *and* BERKMAN, S. 1979. Some comparisons of response and harmonic tide predictions. *International Hydrographic Review*, **56**, 105–15.